The pH effect on PEDOT: PSS/GO as a potential hole transport layer

M. D. Nurhafizah*, Tan You Zi, and B. Afzalina

School of Physics, Universiti Sains Malaysia,
11800 Minden, Penang, Malaysia
**Tel: +60194104058;*
*e-mail:*mdnurhafizah@usm.my*
ORCID: 0000-0003-3660-5274*

Received 29 december 2025; accepted 19 may 2026

Poly(3,4-ethylenedioxythiophene)-polystyrenesulfonate (PEDOT: PSS) with secondary doping has been widely researched as a hole transport layer in solar cells because secondary doping can provide conformational change and improve the properties of PEDOT: PSS. PEDOT: PSS is doped with graphene oxide (GO) to form PEDOT: PSS/GO solution, and then, sodium hydroxide is added into the acidic PEDOT: PSS/GO solution. The novelty of this work relies on the pH effect of PEDOT: PSS/GO, which shows basic condition allows better dispersity of GO in water. The HRTEM result indicates the formation of PEDOT: GO. Besides, the two-point probe results show that both acidic and basic PEDOT: PSS/GO is more conductive than PEDOT: PSS and GO alone. This was due to the transformation of benzoid structure to quinoid structure which has been supported by the lower d-spacings of acidic PEDOT: PSS/GO (3.48 Å) and basic PEDOT: PSS/GO (3.44 Å) compared to PEDOT: PSS (3.56 Å) in the XRD result. Other than that, the UV-Vis absorbance result shows that the PSS chain absorbance peak in basic PEDOT: PSS/GO is around 13% lower than that in acidic PEDOT: GO, indicating better replacement of insulating PSS chain and more successful formation of PEDOT: GO. In the EDX results, the basic PEDOT: PSS/GO shows higher oxygen content (93.34%) than acidic PEDOT: PSS/GO (44.58%) due to the increase of hydroxyl groups of GO in basic conditions caused by NaOH. Besides, the average resistance values of the basic PEDOT: PSS/GO and acidic PEDOT: PSS/GO layers are 3.72E+10 Ω and 1.30E+10 Ω, respectively. The Na^+ ion in NaOH resulted in the damages of unreacted PEDOT: PSS, making the basic PEDOT: PSS/GO sample more electrically resistant than the acidic PEDOT: PSS/GO sample. Despite some of the adverse effects of basic PEDOT: GO, it shows the lowest surface roughness (Rq: 2.52 nm) among all potential HTLs investigated, indicating the best deposition on glass and wettability for organic semiconductors (OSCs) which can be applied as a counter electrode in dye-sensitized solar cell (DSSC) application.

Keywords: Polymer; graphene oxide; acidic; basic; characterization; properties.

DOI: https://doi.org/10.31349/RevMexFis.72.061004

1. Introduction

Organic materials which are low-cost materials have been greatly utilized as third-generation solar cells such as the dye-sensitized solar cells and the perovskite solar cells [1]. The hole transport layer has been an important interlayer in organic solar cells [2] and perovskite solar cells to perform better hole extraction and transportation [3]. According to Yu et al. (2018), one of the very popular hole transport layers used in perovskite solar cells is poly(3,4-ethylenedioxythiophene)-polystyrenesulfonate (PEDOT: PSS) since it can form a smooth surface on the indium-tin oxide (ITO) electrode [4]. Even so, it has disadvantages like being very acidic which could cause corrosion on the perovskite layer and ITO electrode, because of that, the stability and the performance of perovskite solar cells based on PEDOT: PSS hole transport layer (HTL) can be adversely affected [4]. Other than perovskite solar cells, PEDOT: PSS can work as a hole transport layer for organic solar cells as well [5]. The PSS component in PEDOT: PSS is held with the PEDOT unit through an ionic bond and such interaction provides stabilization in aqueous media [6]. Ozcan et al. (2020) mentioned that the good aspect of PSS is that it can make PEDOT: PSS dispersive, however, PSS is insulating, thus, the conductivity of PEDOT: PSS is adversely affected by the PSS component, even so, it is possible to increase the conductivity through secondary doping [6].

One of the very popular types of materials to be combined or doped with PEDOT: PSS is the carbon material such as graphene [7,8], graphene oxide (GO) [9,10], and reduced graphene oxide (rGO) [11,12]. Among various graphene-based materials mentioned, although having conductivity lower than graphene and rGO, GO has the best wettability to deposit perovskite solution [13]. It has been reported that the removal of insulating PSS could increase the conductivity but the power conversion efficiency still decreases because the PEDOT-rich surface is unfavorable for the perovskite crystal growth [14]. The pros of GO for having strong wettability for perovskite deposition could outweigh its cons of being less conductive than graphene and rGO. Since acid is a hygroscopic [15], it can absorb moisture, resulting in poor stability of solar cells [16]. It has been widely known that the highly acidic PEDOT: PSS can degrade the perovskite layer in a perovskite solar cell, as a result, the efficiency and stability

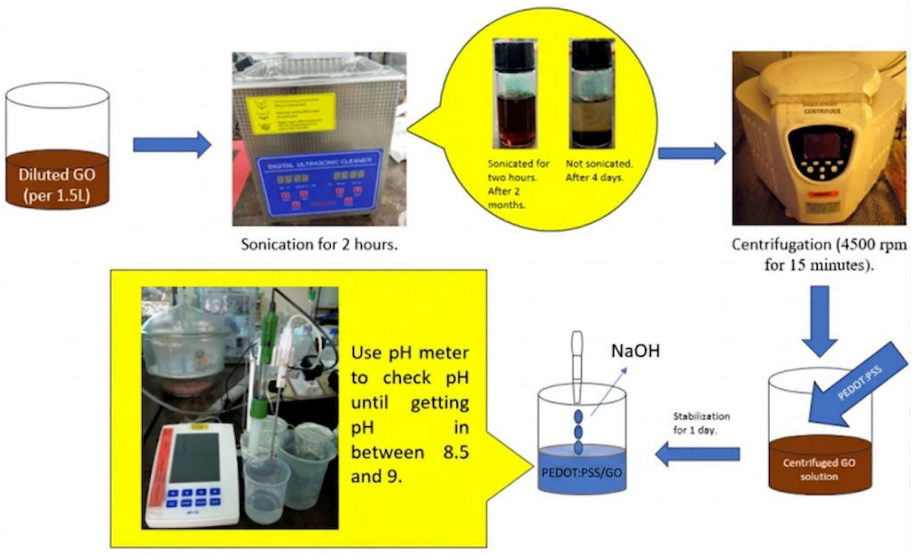


FIGURE 1. Modified synthesis of acidic and basic PEDOT: PSS/GO solutions.

of perovskite solar cells have been greatly reduced [17]. Furthermore, the acidity of PEDOT: PSS can harm the ITO electrode in organic solar cells as well [18]. So, research related to the effect of pH condition on PEDOT: PSS on the performance of perovskite solar cells has been conducted, and basic PEDOT: PSS hole transport layer has indicated better performance in terms of efficiency than the acidic PEDOT: PSS hole transport layer [17] Even so, it has been shown that basic PEDOT: PSS has lower wettability [17], and that can adversely affect the deposition of the perovskite solution in an inverted structure solar cell [19]. Thus, to increase the wettability, the addition of GO is a good choice because GO can increase the wettability of the composite [19]. Coincidently, the basic condition can make GO a more dispersive [20]. GO aggregates in acidic conditions and dissolves better in basic conditions because carboxyl groups of GO can be protonated in acidic conditions and that makes it less hydrophilic, thus forming an aggregation [20]. On the contrary, the carboxyl groups can be deprotonated in a basic condition which makes GO a more dispersive [20], due to the electrostatic repulsion between the deprotonated carboxyl groups [21].

In this study, the pH of basic PEDOT: PSS/GO solution was tuned by NaOH, and different potential hole transport materials which are GO, PEDOT: PSS, acidic, and basic PEDOT: PSS/GO were compared to study the electrical, structural, and optical properties. Besides, the pros and cons of acidic PEDOT: PSS/GO and basic PEDOT: PSS/GO were investigated.

2. Materials and methods

2.1. Sample Preparation

GO was synthesized with graphite (C0350) from HmbG Chemicals through a modified Hummer's method [22]. GO was kept in the solution form without drying into powder form and the solution was diluted to 1.5 L. The conductive grade poly(3,4-ethylenedioxythiophene)-poly(styrenesulfonate) (PEDOT: PSS) with 1.3 wt% dispersion in H_2O (483095-500G) was purchased from Sigma Aldrich. The PEDOT: PSS/GO solution synthesis process was modified from the method conducted by Yu *et al.* (2014) [23]. The graphene oxide solution was sonicated for 2 hours. Then, the sonicated solution was centrifuged at 4500 rpm for 15 minutes to remove any large GO nanosheets, which means the centrifuged solution was kept and the very little precipitate was removed. Next, the PEDOT: PSS solution was mixed with the GO solution directly with the volume ratio of 1: 1 and the mixture was left in the fridge (3°C) to be stabilized for one day. The original PEDOT: PSS/GO solution was acidic (pH between 2 and 2.5). After that, 0.1 M of NaOH was carefully added drop by drop with a dropper to the solution until the solution became basic (pH between 8.5 to 9). The pH meter was used to determine the pH of the solution intermittently until the desired pH. The acidic and basic PEDOT: PSS/GO mixture solutions were spin-coated onto the cleaned glass substrates at 4000 rpm for 45 seconds, then, the layer was annealed at 145°C for 15 minutes [23]. GO and PEDOT: PSS solutions were also deposited with the same procedure for further investigation.

2.2. Material characterizations

To provide a fundamental baseline for PEDOT: PSS/GO solutions, Agilent Technologies: Cary Series UV-Vis-NIR Spectrophotometer was used to obtain the absorbance spectra of various potential hole transport layer using solution-based measurement. The wavelength range scanned was between 200 nm and 800 nm using standard cuvette of 10 mm optical pathlength. High-Resolution Transmission Electron Microscopy (HRTEM) images were obtained by using JEOL JEM 2100F Field Emission Transmission Electron

Microscope (FETEM) operated at an accelerating voltage of 200 kV. Bruker D8 DISCOVER featured with DAVINCI design was employed to obtain the X-ray diffraction (XRD) pattern, the radiation source is Cu-Kα, and 2θ was scanned from 10°C to 90°C. For XRD, the samples were drop-cast rather than spin-coated. The atomic force microscope (Bruker Dimension Edge) was used to study the surface morphology and roughness of the potential hole transport layers. The scan range for each spot was 5 micrometers and the scanning was run at 1 Hz. The spring constant and resonance frequency for the silicon cantilever were around 40 N/m and 250-300 kHz respectively.

A field emission scanning electron microscope (NOVA NANOSEM 450) was employed to obtain high-resolution images of deposited potential HTL particles and the elemental components by the EDX feature. The FESEM images were taken at the voltage of 10 kV with magnification of 10 kX and 100 kX. The EDX feature was run at 10 kV with a working distance of 5 mm and the magnification was 10 kX. KEITHLEY 4200-SCS two-point probe was employed to obtain the current-voltage (I-V) curves of different deposited potential hole transport layers. The working voltage range was -10 V to 10 V and the resistance values could be obtained from 1/gradient of the I-V curves.

3. Results and discussion

3.1. UV-Vis result

As shown in Fig. 2, the absorbance peaks of GO, PEDOT: PSS, basic PEDOT: PSS/GO, and acidic PEDOT: PSS/GO in between the regions of 200 nm to 800 nm are 231 nm, 224 nm, 225 nm, and 225 nm respectively. GO has an absorbance peak at around 231 nm which is very near to the previously reported result [24]. The absorbance peak around 230 nm is due to the electron transition at the carbon π bonds

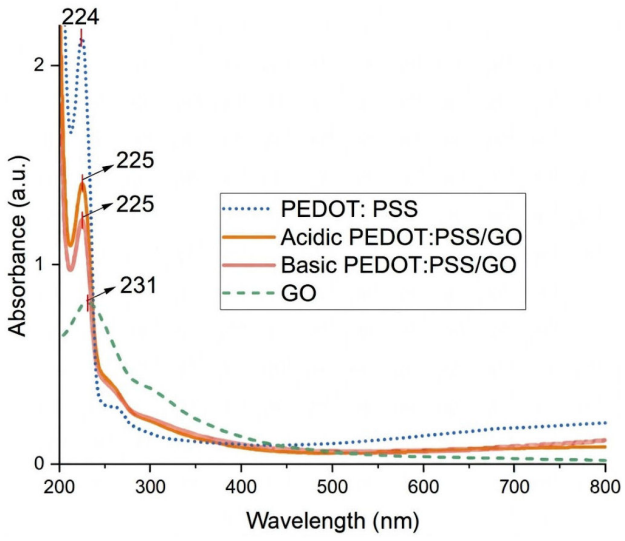


FIGURE 2. Absorbance spectra of potential HTL solutions.

[25]. According to Xia *et al.* (2012), the absorbance peak at around 224 nm is the absorbance peak of the aromatic ring of the PSS unit, thus, the decrement of the peak intensity around that region indicates more replacement of PSS with GO [26]. Based on this concept, it is seen in Fig. 2 that the peak intensity of basic PEDOT: PSS/GO at 225 nm is around 13% lower than that of acidic PEDOT: GO, which shows more replacement of PSS in the basic PEDOT: PSS/GO solution. The reason can be that GO is more dispersive in basic conditions than in acidic conditions [20], thus, GO is more evenly mixed with PEDOT: PSS, so, the replacement of PSS with GO can be more widely done. The PSS chain detached from the PEDOT unit can be attached to GO through the hydrophilic-hydrophilic interaction [27]. Another possible reason behind the lower PSS chain absorbance of basic PEDOT: PSS/GO is that the Na^+ from NaOH can remove PSS from PEDOT: PSS to form Na^+PSS^- [28]. The reason for the red-shift of PSS chain peak from 224 nm in PEDOT: PSS absorbance spectrum to 225 nm in the acidic and basic PEDOT: PSS/GO absorbance spectra is possibly due to the effect of GO, which has a peak at 231 nm rather than 224 nm, thus, slightly red-shifting the peak. However, there was no peak shown at around 231 nm (GO absorbance peak) for both acidic and basic PEDOT: PSS/GO but the presence of a 225 nm peak for the PSS chain is distinct for both cases, which indicates the dominant presence of unreacted PEDOT: PSS in the PEDOT: PSS/GO solutions, although a portion of PEDOT: PSS has been transformed into PEDOT:/GO. This measurement confirms the interaction and mechanism between PEDOT: PSS and GO to produce acidic and basic PEDOT: PSS/GO.

3.2. HRTEM Result

Figure 3 shows the HRTEM images of GO and PEDOT: PSS/GO at different resolutions. The graphene oxide layer deposited can be observed in Fig. 3a). There are certain dark spots found on the GO layer in Fig. 3b) which are the PEDOT molecules bonded with GO. Figure 3d) shows a clearer image of PEDOT (dark) on GO (bright), which is similar to the image of PEDOT within rGO layers in previous literature [29]. The GO HRTEM image with 10 nm resolution is shown in Fig. 3e), which roughly indicates the hexagonal lattice structure of GO. There are also lines representing the crystallites of PEDOT on the GO layer in Fig. 3f), as indicated in the yellow box. The HRTEM result supports the UV-vis result where the UV-vis result shows the replacement of the PSS chain by GO [26] and the HRTEM result indicates the formation of PEDOT: GO.

The X-ray diffraction pattern has also been obtained as indicated in Fig. 4. As shown in Fig. 4, the graphene oxide indicates a peak at 21.325°C which indicates the interlayer spacing of 0.416 nm, which is not in correspondence to the normal GO XRD peak at around 10°C which represents the interlayer spacing of around 0.8 nm [30]. However, the UV-visible result shown in Fig. 2 indicates the GO absorbance peak at 231 nm which indicates the presence of a graphene

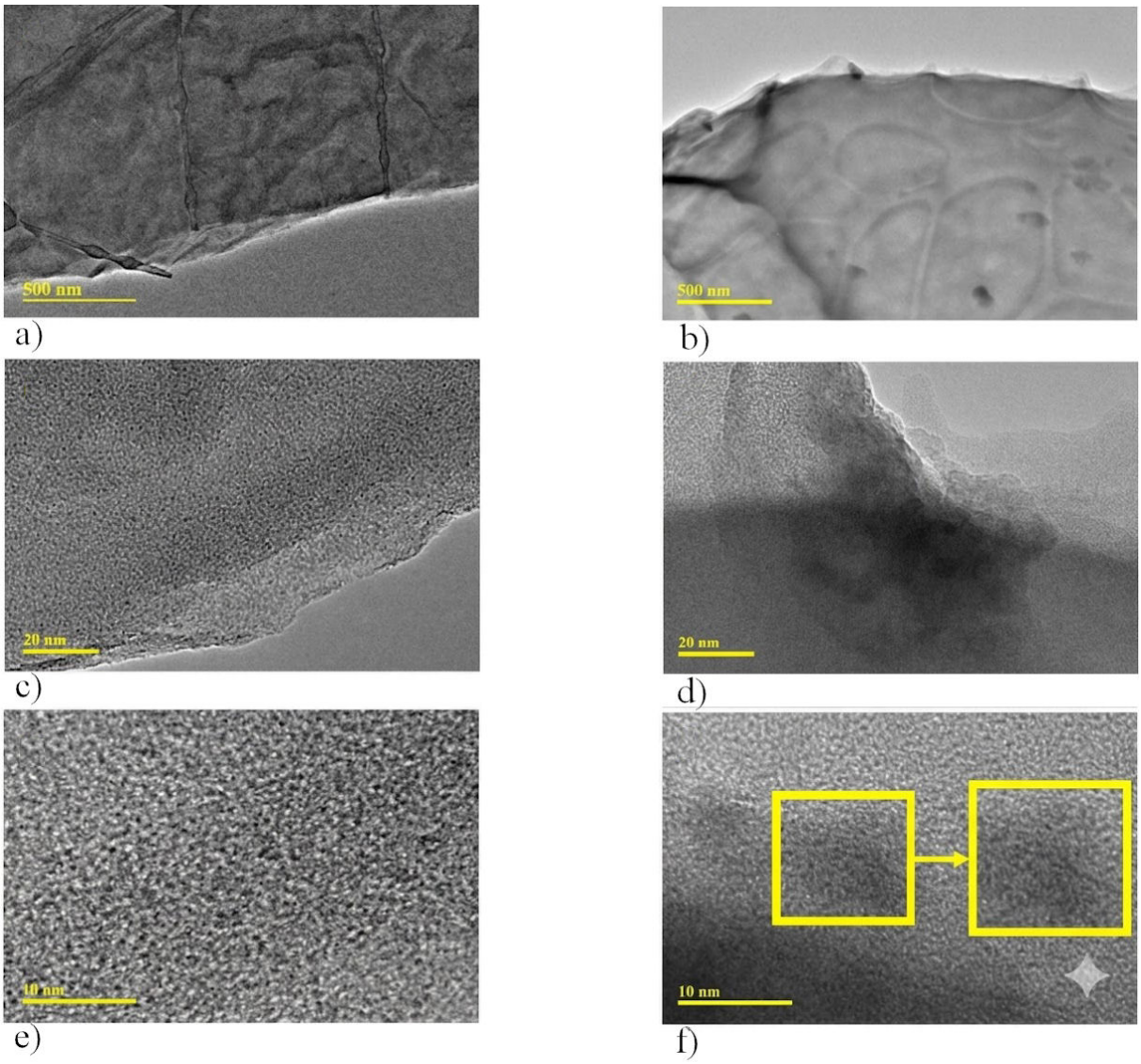


FIGURE 3. HRTEM images of a) GO (500 nm), b) PEDOT: PSS/GO (500 nm), c) GO (20 nm), d) PEDOT: PSS/GO (20 nm); e) GO (10 nm); f) PEDOT: PSS/GO (10 nm).

oxide [24], the reason is probably due to the effect of annealing because the UV-vis absorbance spectra are the results of the hole transport layer (HTL) solutions while the XRD results are obtained after drop-casting and annealing. With more oxygen functional groups, the interlayer spacing increases [31], thus, the lower interlayer spacing obtained shows fewer oxygen functional groups. According to [32], the drying process increases the GO 2θ peak in XRD, where the GO powder dried at 140°C for 30 minutes indicated the 2θ peak between 19 to 24°C because of the eradication of intercalated water and certain oxygen functional groups. Since the annealing temperature in this study is 145°C, the water and oxygen content can be reduced, making the interlayer spacing shorter.

As shown in Fig. 4, the XRD peaks for PEDOT: PSS, acidic PEDOT: GO, and basic PEDOT: PSS/GO are 25°C, 25.553°C, and 25.906°C respectively, indicating the interplanar spacing of 3.56 Å, 3.48 Å and 3.44 Å respectively. The interplanar spacing at around 3.5 Å is the pi-to-pi stacking (010) of PEDOT and the decrease in the pi-to-pi stacking distance can be attributed to the transformation of PEDOT structure from benzoid to quinoid form [33]. The PEDOT bonds with GO through pi-to-pi interactions [34] and for more pi-to-pi interactions to occur [35], the transformation of PEDOT structure from benzoid to quinoid occurs [36]. Because of that, the reduction of interplanar spacing from 3.56 Å to 3.48 Å shows the formation of PEDOT: PSS/GO after GO replaces the PSS chain. This can be supported by the reduction of the PSS chain absorbance peak in the UV absorbance result in Fig. 2 which indicates the replacement of the PSS chain by GO [26] and the HRTEM result in Fig. 3f) which indicates the formation of PEDOT: GO. Thus, lower interplanar spacing of basic PEDOT: PSS/GO (3.44 Å) than that of acidic PEDOT: PSS/GO (3.48Å) indicates more trans-

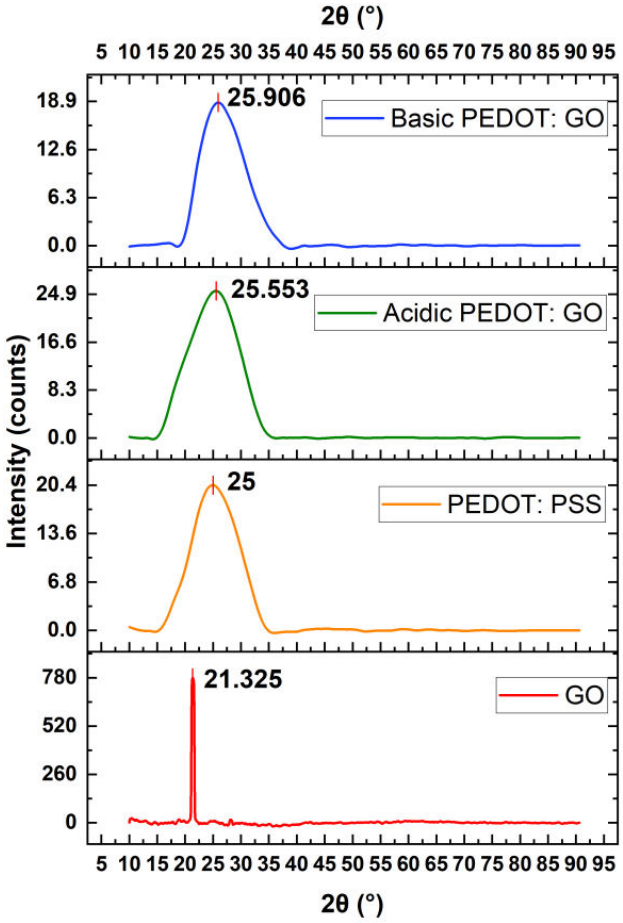


FIGURE 4. X-ray diffraction pattern for basic PEDOT: GO, acidic PEDOT: GO, PEDOT: PSS, and GO.

formation of PEDOT structure from benzoid to quinoid and more PEDOT: PSS/GO formation which corresponds to the lower PSS chain absorbance peak of basic PEDOT: PSS/GO in Fig. 2 that indicates more replacement of PSS chain. In Fig. 4, the GO peak at 21.325 degrees is not observed in the acidic and basic PEDOT: PSS/GO XRD patterns at all, this indicates the low presence of GO. Such phenomenon can be explained by the UV-Vis result in Fig. 2 where the peak of 225 nm which represents the PSS chain absorbance [26] in both acidic and basic PEDOT: PSS/GO is obvious while the GO absorbance peak is unseen. This shows the dominant presence of unreacted PEDOT: PSS even in the PEDOT: PSS/GO solutions.

Figure 5 shows the surface morphology of the four potential hole transport layers. The Rq (root-mean-square) values of two random points on each layer were taken and each average Rq value was calculated. The film thicknesses of PEDOT: PSS, GO, acidic PEDOT: GO, and basic PEDOT: PSS/GO are 32.9 nm, 18.6 nm, 45.0 nm and 49.5 nm, respectively. The surface roughness (Rq) of PEDOT: PSS, GO, acidic PEDOT: GO, and basic PEDOT: PSS/GO are 3.04 nm, 2.65 nm, 2.88 nm, and 2.52 nm, respectively. The low surface roughness result of PEDOT: PSS (3.04 nm) is consistent with the smooth surface characteristic of PEDOT: PSS (less than 5 nm) stated by Sun et al. (2015) [44]. According to Luo et al. (2017), the contact angle of the PEDOT: PSS/GO surface is smaller than the PEDOT: PSS surface, which shows that GO is more hydrophilic than the PSS chain unit [19]. That allows GO and GO-based materials to be deposited more evenly due to the stronger adhesion on glass. Thus, GO and both acidic and basic PEDOT: PSS/GO show lower surface roughness than PEDOT: PSS.

The basic PEDOT: PSS/GO surface with the Rq value of 2.52 nm is smoother than the acidic PEDOT: PSS/GO surface with the Rq value of 2.88 nm. That seems to contrast with the previous result [17], which showed that basic PEDOT: PSS has a higher contact angle than acidic PEDOT: PSS and neutral PEDOT: PSS. However, since the result shown in that literature does not involve GO, it does not take GO dispersity in basic conditions into account. GO is more dispersive in the basic condition [20]. Because of that, GO can spread in the solution more evenly, providing more possibility to react with PEDOT: PSS, thus, allowing more formation of PEDOT: PSS/GO molecules. Since PEDOT: PSS/GO is more hydrophilic than PEDOT: PSS [19], more PEDOT: PSS/GO formation allows the solution to be more hydrophilic. Higher hydrophilicity allows better adhesion on glass, thus, allowing more even deposition, because of that, basic PEDOT: PSS/GO shows lower surface roughness than acidic PEDOT: GO. That can be supported by the UV-vis result in Fig. 2, where the lower PSS chain peak absorbance of basic PEDOT: PSS/GO solution indicates more removal of PSS [26] and the XRD result, where the lower pi-to-pi stacking in basic PEDOT: PSS/GO indicates more benzoid to quinoid transformation [33] and thus, more PEDOT: PSS/GO formation [23].

However, there is also another possible reason for basic PEDOT: PSS/GO to be more dispersive than acidic PEDOT: GO, which is due to the damage of the epoxide group and the production of the hydroxyl group after lengthy mixing with NaOH, resulting in the formation of graphene hydroxide [37]. The epoxide group's contribution to solubility is smaller than the hydroxyl group due to the lower solubility of the R-O-R group than the R-OH group [38]. Thus, the increase of hydroxyl groups in GO makes the overall mixture of basic PEDOT: PSS/GO more dispersive than the mixture of acidic PEDOT: GO, causing better wettability and adhesion on glass, resulting in more even deposition and lower surface roughness. Since a rough surface can lead to interfacial recombination which is undesired in the solar cell application [39], basic PEDOT: PSS/GO with the lowest surface roughness can have the least interfacial recombination.

The elemental evolution of the (HTL) composites was quantitatively assessed via Energy-Dispersive X-ray (EDX) spectroscopy. From Fig. 6a), the analysis of pristine GO revealed a balanced atomic distribution of oxygen (49.22 %) and carbon (50.78 %), whereas pristine PEDOT: PSS showed in Fig. 6b) exhibited a significantly higher oxygen concentration of 85.1 %. This elevated oxygen content is intrinsic to the PEDOT: PSS structure, arising from the oxygen-dense ethylenedioxy groups in the PEDOT backbone and the sul-

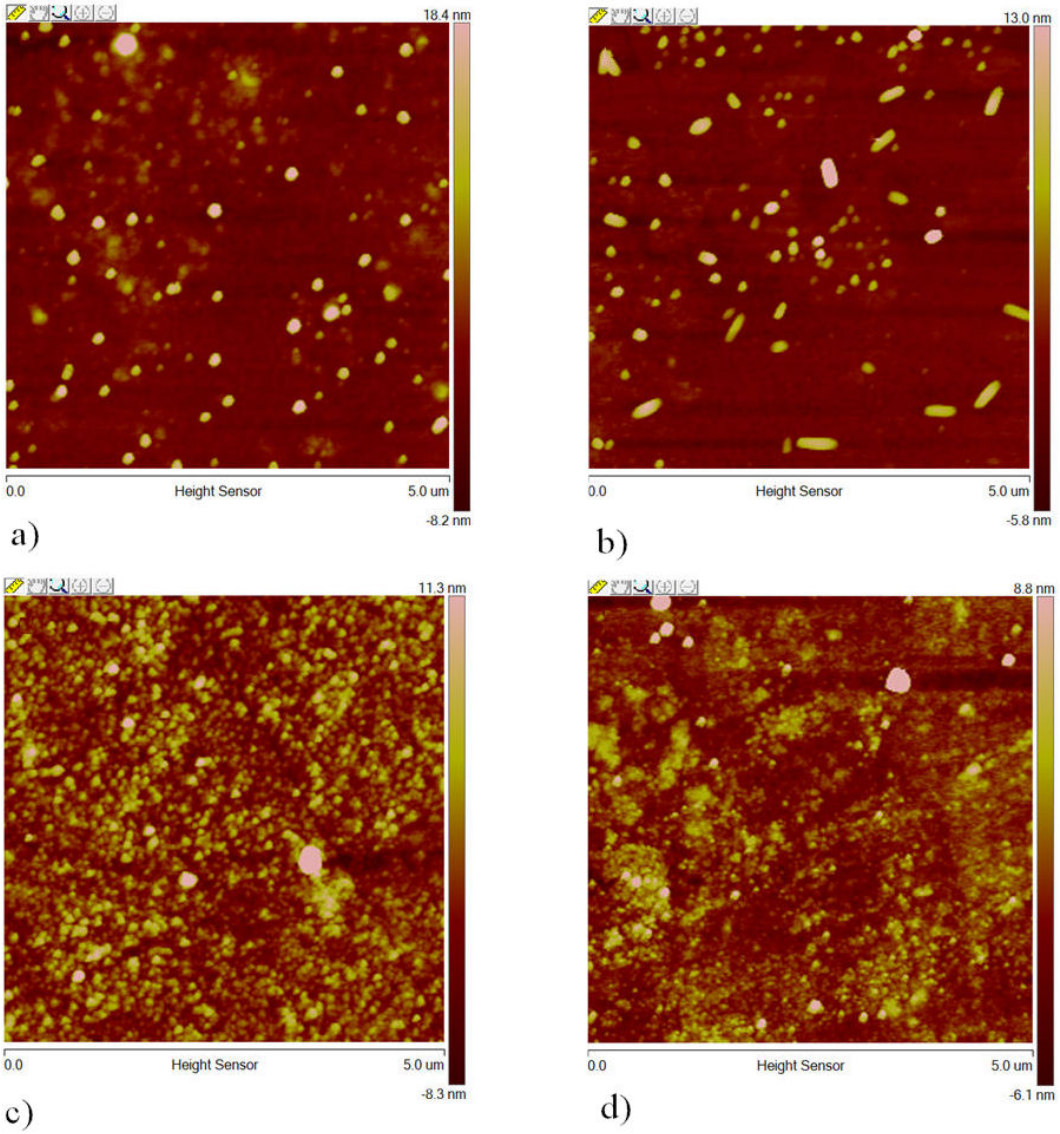


FIGURE 5. Atomic force microscopy results for a) PEDOT: PSS; b) GO; c) acidic PEDOT: GO; d) basic PEDOT: GO.

fonate groups of the PSS chains. Upon the integration of GO to form the acidic PEDOT: PSS/GO composite as in Fig. 6c), the carbon content increased markedly to 55.12 % compared to the 14.21 % observed in pristine PEDOT: PSS. This shift confirms the successful loading of the carbon-dense GO lattice within the polymer matrix. A profound elemental divergence was observed in the basic PEDOT: PSS/GO sample in Fig. 6d), which exhibited an anomalous oxygen concentration of 93.34 % and a depleted carbon fraction of 6.41 %.

This phenomenon is likely driven by two synergistic mechanisms. First, the enhanced dispersity of GO under alkaline conditions promotes more intimate mixing with the PEDOT: PSS matrix, facilitating the displacement of insulating PSS chains [20]. While UV-Vis spectroscopy confirmed a 13 % reduction in PSS absorbance which indicates successful PSS replacement by GO and Na^+ ions [26,28], the magnitude of the oxygen spike suggests a second, more dominant chemical transformation. Under basic conditions, the introduction of NaOH facilitates the ring-opening of the epoxy groups on the GO basal plane, leading to a proliferation of hydroxyl functionalities and the formation of graphene hydroxide species [37]. This chemical restructuring is further supported by the sulfur (S) content trends. The atomic percentage of sulfur decreased from 0.3 % in the acidic composite to 0.24 % in the basic variant. This reduction is attributed to the interaction of Na^+ ions with the PSS^- polyanion, forming Na^+PSS^- complexes that effectively decouple the PSS from the PEDOT: PSS/GO system [28,34]. Since the PSS chains typically maintain stability through hydrogen bonding with the GO oxygen groups, their displacement by Na^+ results in a localized reduction of the sulfur signature. These elemental shifts, combined with the observed reduction in XRD d-spacing from 3.56Å to 3.44Å, underscore a transition from a coiled benzoid to a planarized quinoid con-

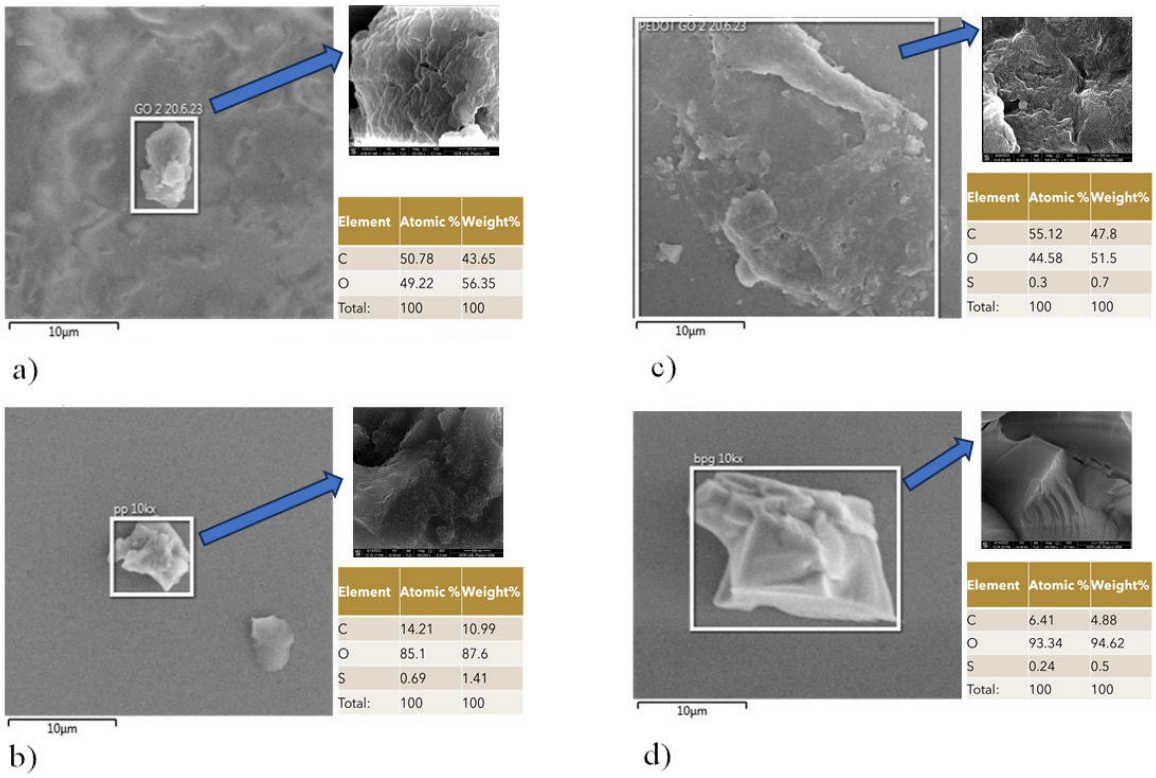


FIGURE 6. FESEM and EDX results at 10kX for a) GO; b) PEDOT: PSS; c) acidic PEDOT: PSS/GO and d) basic PEDOT: GO. Insets are the FESEM images at 100kX.

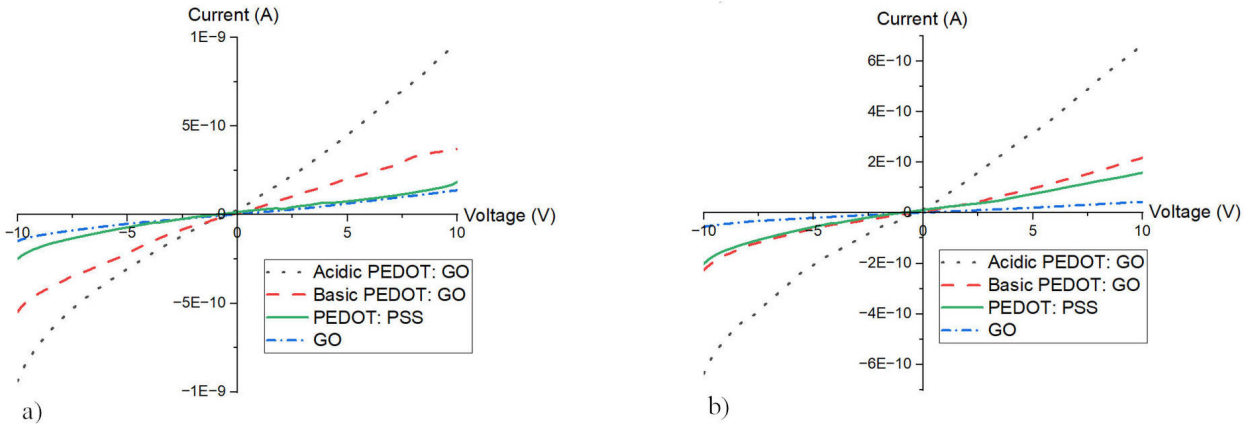


FIGURE 7. Two-point probe results for each HTL; a) random region 1; b) random region 2.

formation, ultimately governing the optoelectronic performance of the resulting HTL.

3.3. I-V result

Figure 7 shows the I-V curves for each HTL at two random regions. The average resistance value for each HTL was calculated and tabulated as shown in Table I. As shown in Fig. 7, GO has the lowest curve among all which means it is the least conductive potential hole transport layer, with the highest average resistance of 1.55E+11 Ω and lowest bulk conductivity of 8.58E-09 S/cm as shown in Table I. Due to the existence of the oxygen functional groups, GO has a low electrical conductivity [40]. PEDOT is a conjugated polymer [41] and its conductivity can be contributed to the conjugated bonds with pi electrons which are delocalized [42]. After PEDOT: PSS reacts with GO, GO replaces the insulating PSS to form PEDOT: GO, and PEDOT combines with GO through the pi-to-pi interaction [34]. During this process, PEDOT transforms from a benzenoid structure to a quinoid structure to allow more pi-to-pi interactions [35,36]. This can be supported by the lower pi-to-pi stacking of basic PEDOT: PSS/GO (3.44Å) and acidic PEDOT: GO (3.48Å) than that of PEDOT: PSS

TABLE I. Average resistance and bulk conductivity for each HTL.

HTL material	Resistance (Ω) First region	Resistance (Ω) Second region	Average Resistance (Ω)	Sheet Resistance (Ω/sq)	Bulk Conductivity, σ(S/cm)
Acidic PEDOT: PSS/GO	1.06E+10	1.54E+10	1.30E+10	1.95E+10	1.03E-07
Basic PEDOT: PSS/GO	2.76E+10	4.69E+10	3.72E+10	5.58E+10	3.58E-08
PEDOT: PSS	5.86E+10	6.79E+10	6.33E+10	9.50E+10	2.11E-08
GO	7.39E+10	2.37E+11	1.55E+11	2.33E+10	8.58E-09

(3.56Å) in the XRD result which reflects the transformation of PEDOT structure from benzoid to quinoid [33]. The increase of pi-to-pi interactions provides more paths for electron transfer [43], facilitating the electron transport process [44], thus, making PEDOT: PSS/GO more conductive than PEDOT: PSS with the values of 3.58E-08 S/cm and 2.11E-08 S/cm respectively. Meanwhile, the acidic PEDOT: PSS/GO and basic PEDOT: GO showed average resistance values of 1.30E+10 Ω and 3.72E+10 Ω showing lower electrically resistance than PEDOT: PSS, which has an average resistance value of 6.33E+10 Ω. Basic PEDOT: PSS/GO shows better conductivity than acidic PEDOT: GO with the value of 2.11E-08 S/cm and 1.03E-07 S/cm respectively. However, the results in Fig. 7 show that basic PEDOT: PSS/GO has a lower I-V curve than acidic PEDOT: GO, thus, it is less conductive than acidic PEDOT: GO.

Moreover, Table I shows that the basic PEDOT: PSS/GO has an average resistance value of 3.72E+10 Ω, which is higher than acidic PEDOT: PSS/GO which has an average resistance value of 1.30E+10 Ω. The PSS chain is significant in stabilizing the PEDOT: PSS molecule, thus, the loss of PSS which destabilizes PEDOT: PSS can adversely affect the charge carrier concentration [45]. When NaOH is present, Na^+ reacts with the PSS chain to form Na^+PSS^- [28], thus, the PEDOT: PSS which loses the PSS component is destabilized. Although many of the PEDOT: PSS have been transformed into PEDOT: PSS/GO in the basic PEDOT: PSS/GO solution, there are unreacted PEDOT: PSS molecules that can contribute to the conductivity as well. In fact, by referring to the absorbance spectra in Fig. 2, the peak of 225 nm which represents the PSS chain absorbance [26] in both acidic and basic PEDOT: PSS/GO is distinct, showing the dominant presence of unreacted PEDOT: PSS. When NaOH is used as a base, the NaOH destroys the unreacted PEDOT: PSS molecules, making them destabilized [28]. Thus, although there are more PEDOT: PSS/GO molecules formed in the basic condition than those formed in the acidic condition, the overall conductivity contributed by both PEDOT: PSS/GO and unreacted PEDOT: PSS is higher in the acidic PEDOT: PSS/GO layer than that in the basic PEDOT: PSS/GO layer, making the basic PEDOT: PSS/GO layer more electrically resistant than the acidic PEDOT: PSS/GO layer.

As compared to commercial ITO electrodes (10–100 Ω/sq); (1.0 x 10^3 S/cm), the optimized Acidic PEDOT: PSS/GO film exhibits a highly resistive profile that is 9 orders of magnitude higher in sheet resistance and 12 orders of magnitude lower in bulk conductivity, a divergence consistent with its role as a charge-selective interface rather than a bulk current collector. Consequently, this multi-order of magnitude difference does not hinder device performance. While the underlying ITO layer is engineered exclusively for low-loss bulk current extraction, these ultra-thin polymer blends are optimized for energy level alignment, targeted hole extraction, and electron blocking at the active layer boundary.

4. Conclusion

In a nutshell, PEDOT: PSS, as a commonly employed hole transport layer can be doped with carbon materials such as graphene oxide to improve its performance. The PEDOT: PSS/GO synthesized from the mixture of PEDOT: PSS and GO has shown better electrical properties, being more conductive than PEDOT: PSS and GO. However, the acidic PEDOT: GO, with a lower average resistance value of 1.30E+10 Ω and conductivity value of 1.03E-07 S/cm is more conductive than the basic PEDOT: PSS/GO which has higher average resistance value of 3.72E+10 Ω due to the damage of unreacted PEDOT: PSS caused by NaOH. Based on the UV-Vis absorbance result, the PSS chain absorbance peak of the basic PEDOT: PSS/GO is around 13% less than that of the acidic PEDOT: GO, indicating more replacement of the PSS chain and better formation of PEDOT: GO. The XRD result further supports the UV-vis result. The basic PEDOT: PSS/GO has lower pi-to-pi stacking (3.44Å) than acidic PEDOT: PSS/GO (3.48Å) which indicates more benzoid to quinoid transformation and more PEDOT: PSS/GO formation in basic PEDOT: GO. The EDX results indicate higher oxygen content in the basic PEDOT: PSS/GO (93.34%) than in the acidic PEDOT: PSS/GO (44.58%) due to the presence of NaOH which generates more hydroxyl groups in GO. Even so, based on the AFM result, the basic PEDOT: PSS/GO still shows the lowest surface roughness (Rq: 2.52 nm) among all potential HTLs, which can lead to the lowest interfacial recombination among all. That is due to the better wettability of basic PEDOT: PSS/GO because of the higher dispersity of GO in basic condition, thus, making the adhesion on glass better. Therefore, the potential usage of basic PEDOT: PSS/GO in the organic semiconductors (OSCs) such as film deposited onto ITO as counter electrode for dye-sensitized solar cell (DSSC).

Acknowledgment

The authors would like to express their profound gratitude for the financial support received from the Ministry of Higher Education Malaysia for Fundamental Research Grant Scheme with Project Code: (FRGS/1/2022/STG07/USM/02/8), and the Bridging Grant (RUI), USM (grant number: R501-LR-RND003-0000002174-0000).

Authors contribution

M.D. Nurhafizah: Writing-original draft; supervision; resources
Tan You Zi: Methodology, formal analysis
B. Afzalina: Writing-review and editing, formal analysis

Conflict of interest

There is no conflict of interest.

1. S. Katoon *et al.*, Perovskite solar cell's efficiency, stability and scalability: A review, *Materials Science for Energy Technologies* **6** (2023) 437, https://doi.org/10.1016/j.mset.2023.04.007
2. H. Xu *et al.*, Hole transport layers for organic solar cells: recent progress and prospects, *Journal of Materials Chemistry A* **8** (2020) 11478, https://doi.org/10.1039/d0ta03511d
3. S. Li *et al.*, A brief review of hole transporting materials commonly used in perovskite solar cells, *Rare Metals* **40** (2021) 2712, https://doi.org/10.1007/s12598-020-01691-z
4. J.C. Yu *et al.*, Highly efficient and stable inverted perovskite solar cell employing PEDOT:GO composite layer as a hole transport layer, *Scientific Reports* **8** (2018) 1070, https://doi.org/10.1038/s41598-018-19612-7
5. Y. Wang *et al*., High-performance hole transport layer based on WS_2 doped PEDOT: PSS for organic solar cells, *Organic Electronics* **99** (2021) 106305, https://doi.org/10.1016/j.orgel.2021.106305
6. S. Ozcan *et al*., Graphene oxide-doped PEDOT: PSS as hole transport layer in inverted bulk heterojunction solar cell, *Journal of Materials Science: Materials in Electronics* **31** (2020) 3576, https://doi.org/10.1007/s10854-020-02906-w
7. W. Li *et al.*, Boost the performance of inverted perovskite solar cells with PEDOT: PSS/Graphene quantum dots composite hole transporting layer, *Organic Electronics* **78** (2020) 105575, https://doi.org/10.1016/j.orgel.2019.105575
8. C. Redondo-Obispo *et al*., Enhanced stability and efficiency in inverted perovskite solar cells through graphene doping of PEDOT: PSS hole transport layer, *Materials & Design* **191** (2020) 108587, https://doi.org/10.1016/j.matdes.2020.108587
9. D.-Y. Lee, S.-I. Na, and S.-S. Kim, Graphene oxide/PEDOT: PSS composite hole transport layer for efficient and stable planar heterojunction perovskite solar cells, *Nanoscale* **8** (2016) 1513, https://doi.org/10.1039/C5NR05271H
10. J. Niu *et al.*, Graphene-oxide doped PEDOT: PSS as a superior hole transport material for high-efficiency perovskite solar cell, *Organic Electronics* **48** (2017) 165, https://doi.org/10.1016/j.orgel.2017.05.044
11. A. Giuri *et al.*, UV Reduced Graphene Oxide PEDOT: PSS Nanocomposite for Perovskite Solar Cells, *IEEE Transactions on Nanotechnology* **15** (2016) 725, https://ieeexplore.ieee.org/abstract/document/7398111/
12. S. Wang *et al*., Hybrid UV-Ozone-Treated rGO-PEDOT: PSS as an Efficient Hole Transport Material in Inverted Planar Perovskite Solar Cells, *Nanoscale Research Letters* **12** (2017) 619, https://doi.org/10.1186/s11671-017-2393-1
13. X. Huang *et al.*, Moderately reduced graphene oxide/PEDOT: PSS as hole transport layer to fabricate efficient perovskite hybrid solar cells, *Organic Electronics* **39** (2016) 288, https://doi.org/10.1016/j.orgel.2016.10.013
14. X.-Y. Li *et al*., The solvent treatment effect of the PEDOT: PSS anode interlayer in inverted planar perovskite solar cells, *RSC Advances* **6** (2016) 24501, https://doi.org/10.1039/c5ra25787e
15. C. Peng, M.N. Chan, and C.K. Chan, The Hygroscopic Properties of Dicarboxylic and Multifunctional Acids: Measurements and UNIFAC Predictions, *Environmental Science & Technology* **35** (2001) 4495, https://doi.org/10.1021/es0107531
16. R. Tariq Ahmedhamdi *et al.*, Humidity impact on photovoltaic cells performance: *A review*, **35** (2018), http://www.ijrerd.com/papers/v3-i11/5-IJRERD-C264.pdf
17. Q. Wang *et al.*, Modulation of PEDOT: PSS pH for Efficient Inverted Perovskite Solar Cells with Reduced Potential Loss and Enhanced Stability, *ACS Applied Materials & Interfaces* **8** (2016) 32068, https://doi.org/10.1021/acsami.6b11757
18. F.J. Lim *et al*., Influence of a novel fluorosurfactant modified PEDOT: PSS hole transport layer on the performance of inverted organic solar cells, *Journal of Materials Chemistry* **22** (2012) 25057, https://doi.org/10.1039/C2JM34484K
19. H. Luo *et al*., Efficient and Air-Stable Planar Perovskite Solar Cells Formed on Graphene-Oxide-Modified PEDOT: PSS Hole Transport Layer, *Nano-Micro Letters* **9** (2017) 39, https://doi.org/10.1007/s40820-017-0140-x
20. C.-J. Shih *et al.*, Understanding the pH-Dependent Behavior of Graphene Oxide Aqueous Solutions: A Comparative Experimental and Molecular Dynamics Simulation Study,

Langmuir **28** (2012) 235, https://doi.org/10.1021/la2036079

21. J.L. Suter and P.V. Coveney, Principles governing control of aggregation and dispersion of aqueous graphene oxide, *Scientific Reports* **11** (2021) 22460, https://doi.org/10.1038/s41598-021-01643-4
22. E.H. Sujiono *et al*., Graphene oxide based coconut shell waste: synthesis by modified Hummers method and characterization, *Heliyon* **6** (2020) e04568, https://doi.org/10.1016/j.heliyon.2020.e04568
23. J.C. Yu *et al*., Highly Efficient Polymer-Based Optoelectronic Devices Using PEDOT: PSS and a GO Composite Layer as a Hole Transport Layer, *ACS Applied Materials & Interfaces* **6** (2014) 2067, https://doi.org/10.1021/am405231b
24. T.F. Emiru and D.W. Ayele, Controlled synthesis, characterization and reduction of graphene oxide: A convenient method for large scale production, *Egyptian Journal of Basic and Applied Sciences* **4** (2017) 74, https://doi.org/10.1016/j.ejbas.2016.11.002
25. V.B. Mbayachi *et al.*, Graphene synthesis, characterization and its applications: A review, *Results in Chemistry* **3** (2021) 100163, https://doi.org/10.1016/j.rechem.2021.100163
26. Y. Xia, K. Sun, and J. Ouyang, Highly conductive poly(3,4-ethylenedioxythiophene):poly(styrene sulfonate) films treated with an amphiphilic fluoro compound as the transparent electrode of polymer solar cells, *Energy & Environmental Science* **5** (2012) 5325, https://doi.org/10.1039/c1ee02475b
27. F.-P. Du *et al.*, PEDOT: PSS/graphene quantum dots films with enhanced thermoelectric properties via strong interfacial interaction and phase separation, *Scientific Reports* **8** (2018) 6441, https://doi.org/10.1038/s41598-018-24840-y
28. T.-C. Tsai *et al*., A facile dedoping approach for effectively tuning thermoelectricity and acidity of PEDOT: PSS films, *Organic Electronics* **15** (2014) 641, https://doi.org/ https://doi.org/10.1016/j.orgel.2013.12.023
29. F. Abd-Wahab, H.F. Abdul Guthoos, and W.W.A. Wan Salim, Solid-State rGO-PEDOT: PSS Transducing Material for Cost-Effective Enzymatic Sensing, *Biosensors* **9** (2019) 6, https://doi.org/10.3390/bios9010036
30. G. Surekha *et al*., FTIR, Raman and XRD analysis of graphene oxide films prepared by modified Hummers method, *Journal of Physics: Conference Series* **1495** (2020) 012012, https://doi.org/10.1088/1742-6596/1495/1/012012
31. N.G. de Barros *et al.*, Graphene Oxide: A Comparison of Reduction Methods, C **9** (2023) 73, https://doi.org/10.3390/c9030073
32. S.B. Singh and S.A. Dastgheib, Physicochemical transformation of graphene oxide during heat treatment at 110-200°, *Carbon Trends* **10** (2023) 100251, https://doi.org/10.1016/j.cartre.2023.100251
33. X. Wang *et al*., Enhancement of thermoelectric performance of PEDOT: PSS films by post-treatment with a superacid, *RSC Advances* **8** (2018) 18334, https://doi.org/10.1039/c8ra02058b
34. R.K. Sharma *et al*., Graphene oxide modified PEDOT: PSS as an efficient hole transport layer for enhanced performance of hybrid silicon solar cells, *Surfaces and Interfaces* **36** (2023) 102577, https://doi.org/10.1016/j.surfin.2022.102577
35. B. Piro *et al*., Fabrication and Use of Organic Electrochemical Transistors for Sensing of Metabolites in Aqueous Media, *Applied Sciences* **8** (2018) 928, https://doi.org/10.3390/app8060928
36. J. Ouyang *et al*., On the mechanism of conductivity enhancement in poly(3,4-ethylenedioxythiophene):poly(styrene sulfonate) film through solvent treatment, *Polymer* **45** (2004) 8443, https://doi.org/10.1016/j.polymer.2004.10.001
37. D. Lee and J. Seo, Three-dimensionally networked graphene hydroxide with giant pores and its application in supercapacitors, *Scientific Reports* **4** (2014) 7419, https://doi.org/10.1038/srep07419
38. V.V. Neklyudov *et al*., New insights into the solubility of graphene oxide in water and alcohols, *Physical Chemistry Chemical Physics* **19** (2017) 17000, https://doi.org/10.1039/C7CP02303C
39. J. Eun Song *et al*., A Thin In_2S_3 Interfacial Layer for Reducing Defects and Roughness of $Cu_2ZnSn(S,Se)_4$ Thin-Film Solar Cells, *Chem.Sus.Chem.* **15** (2022) e202102350, https://doi.org/10.1002/cssc.202102350
40. T. Tene *et al*., Optical properties of graphene oxide, Frontiers in *Chemistry* **11** (2023) 1152865, https://doi.org/10.3389/fchem.2023.1214072
41. T. Kim *et al*., Highly conductive PEDOT: PSS with enhanced chemical stability, *Organic Electronics* **74** (2019) 77, https://doi.org/ https://doi.org/10.1016/j.orgel.2019.06.033
42. S.A. Umoren, M.M. Solomon, and V.S. Saji, Chapter 19 - Conducting polymers, in Polymeric Materials in Corrosion Inhibition, S.A. Umoren, M.M. Solomon, and V.S. Saji, *Editors.* **2022** (2022) 443, https://doi.org/10.1016/C2020-0-00555-4
43. G. Skorupskii *et al*., Electrical conductivity through π–π stacking in a two-dimensional porous gallium catecholate metal–organic framework, *Annals of the New York Academy of Sciences* **1518** (2022) 226, https://doi.org/10.1111/nyas.14867
44. B. Sun *et al.*, Electron Transfer Facilitated by π–π Stacking during the Nitrobenzene Recognition Process of an MOF Sensor, *The Journal of Physical Chemistry C* **125** (2021) 12433, https://doi/10.1021/acs.jpcc.1c02942%20
45. S.H. Kim, Control of the Charge Carrier Concentration and Hall Mobility in PEDOT: PSS Thermoelectric Films, *Bulletin of the Korean Chemical Society* **38** (2017) 1460, https://doi.org/10.1002/bkcs.11327